

# Kinematic dilation during the hydraulic stimulation of pre-fractured rocks

S. ROSHANKHAH\*, L. G. CRUZ†, H. SHIN‡, A. LIZCANO§ and J. C. SANTAMARINA||

A single planar fracture geometry dominates the process of hydraulic fracturing in homogeneous, isotropic and cohesive materials. However, this fracture geometry cannot explain the high recovery efficiency observed in shale gas and enhanced geothermal energy. Experimental and numerical studies reported here demonstrate that pre-fractured, structured reservoirs experience extensive geometric distortion and dilation around the main opening-mode discontinuity generated by high-pressure fluid injection. This kinematic dilation may decrease at high confining stresses because blocks deform and split. Parameters such as the dominant fracture set orientation, block size and slenderness and blocks overlap length characterise a pre-structured medium and determine its deformation pattern and hydromechanical behaviour. Kinematically controlled dilational distortion greatly improves fluid conductivity in the pre-structured medium. A sixth-power relationship is anticipated between the enhanced hydraulic conductivity and the roundness of the main opening.

**KEYWORDS:** laboratory tests; monitoring; numerical modelling

ICE Publishing: all rights reserved

## NOTATION

$c_{v\text{-frac}}$	coefficient of pressure diffusion in the fracture ( $m^2/s$ )
$E$	Young's modulus ( $N/m^2$ )
$e$	opening width or crack aperture (m)
$e_0$	initial opening width (m)
$H_b$	block height (m)
$i$	block layer number
$k_b$	hydraulic conductivity of the rock block (m/s)
$k_{hyd}$	hydraulic conductivity (m/s)
$k_{hyd}^0$	initial hydraulic conductivity (m/s)
$k_N$	normal stiffness of the interface elements ( $N/m^2$ )
$k_S$	shear stiffness of the interface elements ( $N/m^2$ )
$L_b$	block length (m)
$L_F$	length of the main opening (m)
$N$	number of blocks composing the main opening
$O_F$	width of the main opening (m)
$p$	fluid pressure ( $N/m^2$ )
$s$	inter-block overlap length (m)
$T$	dimensionless time
$t$	time (s)
$z_i$	distance between top of $i$ -th block layer and the bottom base (m)
$z_1$	distance between top of the first block layer and the bottom base (m)
$\alpha$	constant
$\beta$	angle between the wing opening and the horizontal axis (deg)
$\gamma$	fluid unit weight ( $N/m^3$ )
$\gamma_b$	rock block unit weight ( $N/m^3$ )
$\Delta e$	change in the opening width (m)
$\Delta L$	change in the opening length (m)

$\Delta z_i$	change in the distance between top of $i$ -th block layer and the bottom base (m)
$\Delta z_1$	change in the distance between top of the first block layer and the bottom base (m)
$\eta$	fluid viscosity ( $N\cdot s/m^2$ )
$\lambda$	block aspect ratio ( $\lambda = L_b/H_b$ )
$\sigma_{x\infty}$	far-field horizontal stress ( $N/m^2$ )
$\sigma'_{z0}$	initial vertical stress ( $N/m^2$ )
$\sigma_{z\infty}$	far-field vertical stress ( $N/m^2$ )
$\phi$	internal friction angle (deg)
$\chi$	angle between contiguous points on opposite faces of wing openings (deg)

## INTRODUCTION

Hydraulic fracturing is commonly used to enhance resource recovery from oil, gas and geothermal reservoirs (e.g. Economides & Nolte, 2000; Jeffrey *et al.*, 2010), for deep waste injection (e.g. Delaguna, 1966; Tsang *et al.*, 2015), and to assess the in situ state of stress (e.g. Haimson & Fairhurst, 1969; Zoback *et al.*, 2003; Lakirouhani *et al.*, 2016).

Extensive studies have been conducted to understand the evolution of hydraulic fractures in various geomaterials. Cohesive intact rocks experience a single bi-wing planar fracture; the fluid pressure required to propagate these fractures reflects the rock tensile strength, the in situ stress and pore pressure (Hubbert & Willis, 1957; Detournay, 2016). In addition, frictional granular materials develop opening-mode discontinuities when either viscous drag or capillary forces overwhelm the skeletal forces created by the far-field effective stress (Shin & Santamarina, 2008). There is also the case of pre-existing fractures, where most studies have focused on the interaction between the propagating hydraulic fracture and a single pre-existing fracture in a homogeneous medium (Zoback *et al.*, 1977; Lam & Cleary, 1984; Warpinski & Teufel, 1987; Teufel & Clark, 1984; Cheng *et al.*, 2015); in this case, the system response depends on factors such as the approach angle, the in situ state of stress, rock fracture toughness, fracture friction and aperture, permeability of the rock matrix and fluid injection rate and viscosity (e.g. Lamont & Jessen, 1963; Daneshy, 1974;

Manuscript received 27 September 2018; first decision 8 May 2019; accepted 9 May 2019.

\*California Institute of Technology, 1200 E. California Blvd., MC 104-44, Pasadena, CA 91125, USA (Orcid:0000-0002-1160-7882).

†University of the Cauca, Popayan, Colombia.

‡University of Ulsan, Ulsan, South Korea.

§SRK Consulting, Vancouver, Canada.

||KAUST, Thuwal 23955-6900, Kingdom of Saudi Arabia.

Thiercelin *et al.*, 1987; Cooke & Underwood, 2001; De Pater & Beugelsdijk, 2005; Zhou *et al.*, 2008; Zhang *et al.*, 2009; Wasantha & Konietzky, 2016; Wang, 2017).

Hydraulic fracture formation and growth in pre-structured media such as a fully fractured blocky rock mass remain less understood (Last & Harper, 1990; Gale *et al.*, 2007; NAE, 2015; Lee *et al.*, 2015). Field observations and microseismic measurements hint to the strong influence of pre-existing fractures and the development of complex fracture patterns during hydraulic stimulation of pre-fractured media (Warpinski *et al.*, 2009; Dahi-Taleghani & Olson, 2011; Ren *et al.*, 2016). Furthermore, the predicted stimulated volume does not agree with either the volume inferred from microseismicity or from well production rates (Mayerhofer *et al.*, 2011; Maxwell *et al.*, 2011; Nagel *et al.*, 2013). The generation and propagation of hydraulic fractures in a pre-structured medium must reflect the coupling between the in situ state of stress, geometric characteristics of the formation (block size, slenderness and overlap) and its global hydro-mechanical response, including opening-dependent fluid conductivity, slippage, interlocking and dilation.

This study combines laboratory experiments and coupled hydro-mechanical numerical simulations to elucidate the processes responsible for the response of structured blocky media subjected to hydraulic stimulation. In particular, the study explores the role of the rock internal structure on kinematic dilation away from the main opening.

## EXPERIMENTAL PROCEDURE AND RESULTS

The fractured medium tested in this study consists of an assembly of impermeable, equal-size acrylic blocks ( $25.4 \times 13 \times 13 \text{ mm}^3$ ). Tests involve two different internal structures with inter-block overlap ratios  $s/L_b = 0.5$  and  $0.9$ ,

where  $L_b$  is the block length and  $s$  is the overlap length (Fig. 1).

### Boundary conditions

The block layers rest on a rigid base, and two transparent rigid plates hold the blocky specimen (back and front). Test series involve two extreme lateral boundary conditions: constant zero lateral stress, and zero lateral deformation. The top boundary is free in all cases.

### Procedure

A local displacement is imposed on a selected fracture or block(s) in the bottom layer. The displacement rate is  $0.5 \text{ mm/s}$  for a maximum displacement of  $13 \text{ mm}$ . The recorded data include the displacement field using high-resolution time-lapse photography and the upward force required to stimulate the medium.

### Results

Figure 1 presents selected photographs gathered during loading and unloading stages. The blocky mass experiences extensive dilational distortion away from the imposed displacement at the bottom boundary. Fabric distortions reflect the internal block structure and boundary conditions. Upward propagating wing openings bound most of the far-field distortion and define the stimulated reservoir volume for the fabric with small interblock overlap. Columnar structures form when blocks are stacked with a large overlap ratio.

Irreversible residual deformations remain locked-in on unloading (Fig. 1 – unloading columns). This form of ‘self-propping’ results from blocks that slip under neighbouring blocks (i.e. kinematic propping), or frictionally trapped

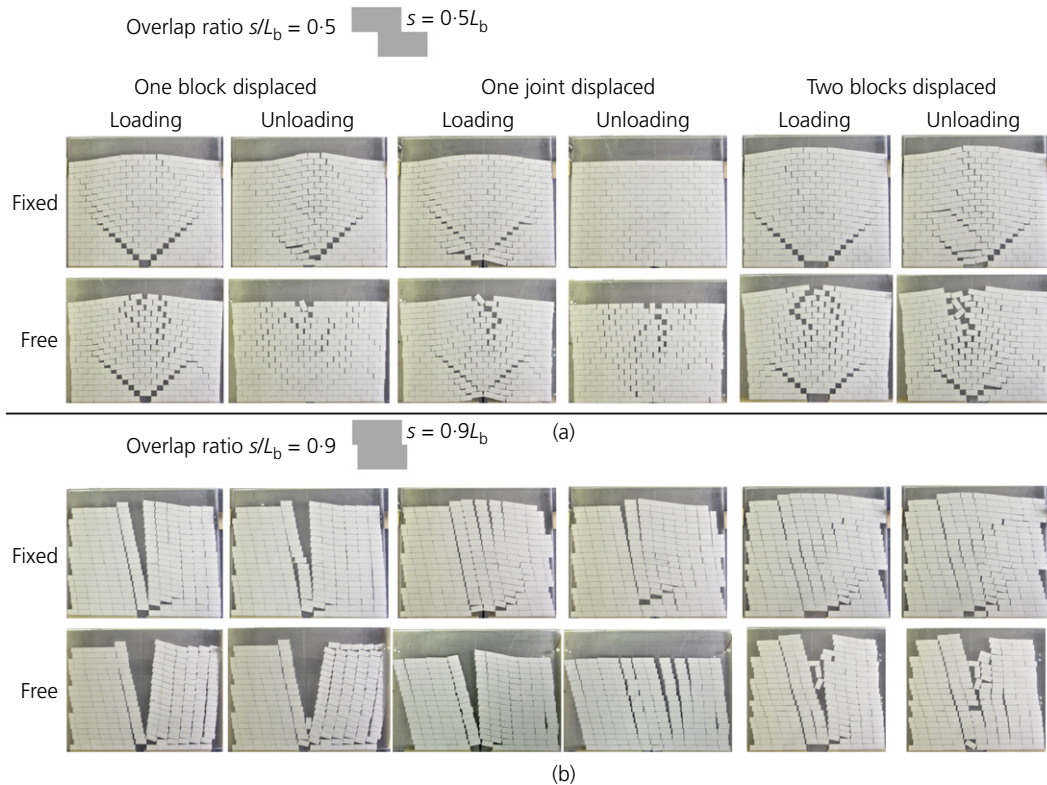


**Fig. 1.** Configuration of the experimental model. Observed dilational distortion during loading and unloading for various cases of imposed displacement: on a block, on a fracture and on two blocks at the bottom layer. Results are shown for two internal structures, with overlap ratios of (a)  $s/L_b = 0.5$  and (b)  $s/L_b = 0.9$ , under fixed and free lateral boundary conditions. Two white tapes are attached on the lateral confining boundaries for reference

block misalignment (i.e. static propping). Self-propping implies block rotation-and-slip, and dilation of the fractured medium (see also Riahi *et al.*, 2014; Lei *et al.*, 2015; Garcia *et al.*, 2018). The high efficiency of proppant-free or waterfrac field treatments confirms self-propping effects as well (Mayerhofer *et al.*, 1997; Chen *et al.*, 2000; Hossain *et al.*, 2002).

Figure 2(a) shows the block vertical displacement  $\Delta z_i$  obtained from digital image analyses at successive  $i$ -th layers away from the main opening plotted against the layer number  $i = z_i/H_b$ ; for comparison,  $\Delta z_i$  data are normalised by the displacement imposed on the first layer  $\Delta z_1$ . The increase in vertical displacement away from the source reflects the gradual accumulation of dilational distortions that occur in each layer.

Force–displacement data collected during these tests exhibit a hysteretic, elasto-plastic response (Fig. 2(b)). The force required to displace a single block is 5–10 times the overburden weight above the displaced block. Higher values apply to the structure with small overlaps due to the increased transverse block interlocking.

## NUMERICAL SIMULATIONS AND RESULTS

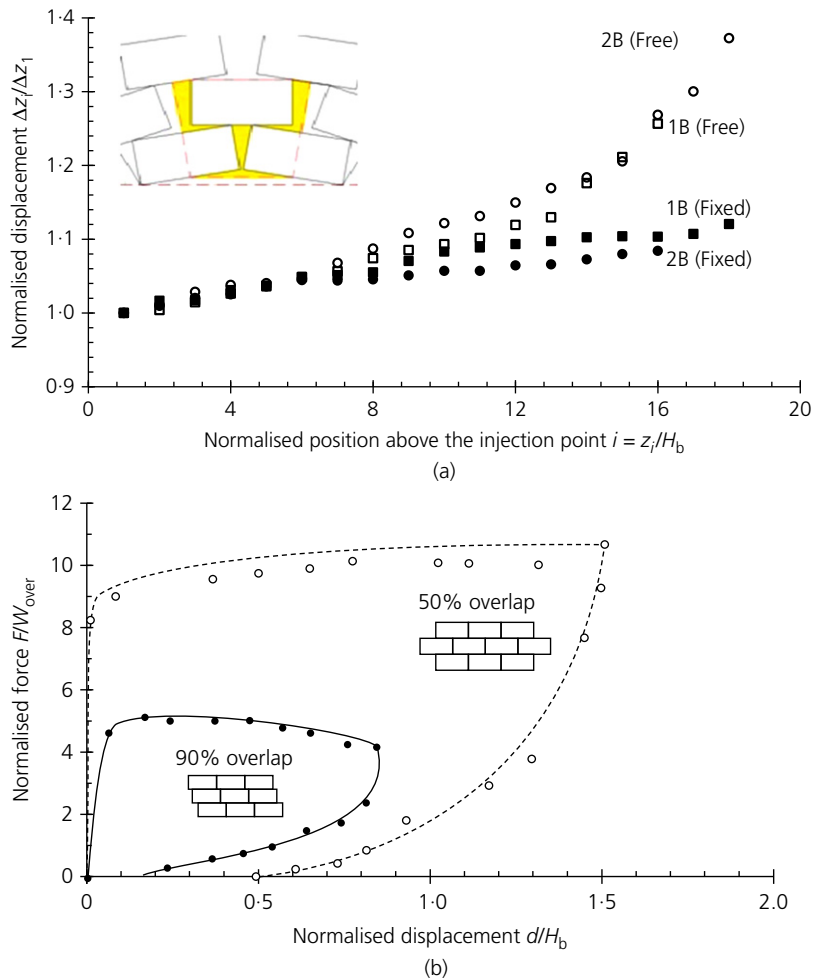
The simulation study uses finite elements to represent both blocks and fractures in the pre-fractured medium. The formulation is fully coupled in terms of deformations,

effective stress and fluid pressure. The two-dimensional orthogonal structured medium is similar to the laboratory specimens described earlier: horizontal layering, block slenderness  $L_b/H_b = 2$ , inter-block overlap ratio  $s/L_b = 0.5$  and plane-strain condition. The structured medium consists of 651 blocks placed in 20 layers (19 200 block elements, 6840 interface elements and 72 510 nodes).

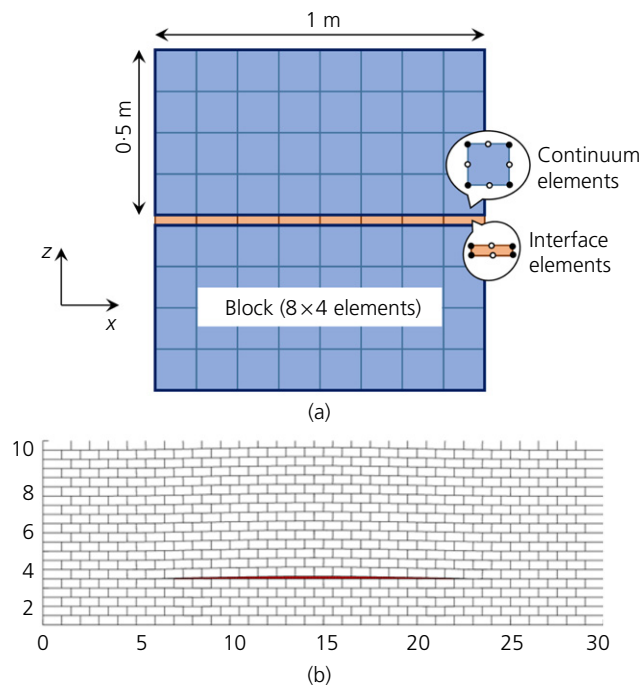
### Algorithm

Figure 3(a) shows two blocks, each discretised into  $8 \times 4$  continuum elements. Each block element has eight nodes for displacement (solid and empty nodes) and four nodes for fluid pressure (solid nodes). Figure 3(a) also shows a fracture discretised to  $8 \times 1$  interface elements. Interface elements consist of six nodes for displacement and four nodes for pore pressure. Interface and block elements share displacement and fluid pressure nodes. Displacement and fluid pressure fields satisfy force equilibrium and fluid mass balance (Galerkin formulation). The fully coupled hydro-mechanical formulation involves a semi-implicit time integration with a Newton–Raphson iterative approach.

All elements are pervious and linear elastic. Interface elements have normal and shear stiffness, and friction. The normal stiffness  $k_N$  is constant in compression. Note that a minimal value of normal stiffness is maintained for numerical stability when blocks separate. Fractures shear with a constant



**Fig. 2.** Experimental simulation results. (a) Measured layer displacement normalised by the displacement of the main opening,  $\Delta z_i/\Delta z_1$ , against position above the injection point normalised by the block height – that is, the layer number:  $i = z_i/H_b$ , before unloading. Test conditions: displacement imposed on one block (1B) or two blocks (2B) under either free or fixed lateral boundaries. (b) Force–displacement data. Force required to displace one block normalised by the weight of the overburden,  $F/W_{over}$ , against the imposed vertical displacement normalised by the block height,  $d/H_b$ .



**Fig. 3.** Configuration of the numerical model. (a) Two two-dimensional rock blocks ( $1 \times 0.5 \text{ m}^2$ ) separated by a fracture. Each pervious and elastic block is represented by  $8 \times 4$  continuum elements; solid and empty nodes are used for deformation, but only solid nodes are used for pore pressure. (b) The pre-structured medium is represented by 651 blocks placed in 20 layers. The fluid injection starts at the centreline on a fracture between the fifth and the sixth block layers

shear stiffness  $k_S$  until they reach the Coulombian frictional resistance characterised by the friction angle  $\phi$ .

Fluid flux through all elements follows Darcy's law. The hydraulic conductivity is constant in blocks. However, the hydraulic conductivity  $k_{\text{hyd}}$  (m/s) through the fracture elements is proportional to the fracture aperture  $e$  (m) at each point along the fracture

$$k_{\text{hyd}} = k_{\text{hyd}}^0 \left( 1 + \frac{\Delta e}{e_0} \right)^\alpha \quad (1)$$

The initial hydraulic conductivity  $k_{\text{hyd}}^0$  (m/s) and initial fracture aperture  $e_0$  (m) are constant throughout the medium at the beginning of the simulation, and the  $\alpha$ -exponent is fixed at 3.0 (Barton *et al.*, 1985; Segura & Carol, 2008; Souley *et al.*, 2015). The fracture aperture  $e$  evolves as part of the numerical solution. Table 1 summarises material parameters and initial conditions.

**Table 1.** Material parameters and initial conditions for the numerical simulations

Blocks:	
Length	$L_b = 1.0 \text{ m}$
Height	$H_b = 0.5 \text{ m}$
Unit weight	$\gamma_b = 20 \text{ kN/m}^3$
Stiffness	$E = 10^6 \text{ kPa}$
Hydraulic conductivity	$k_b = 10^{-6} \text{ m/s}$
Fractures:	
Normal stiffness	$k_N = 10^7 \text{ kN/m}$ in compression $k_N = 10^{-2} \text{ kN/m}$ in tension
Shear stiffness	$k_S = 10 \text{ kN/m}$
Friction angle	$\phi = 30^\circ$
Initial fracture opening	$e_0 = 1.0 \text{ mm}$
Initial hydraulic conductivity	$k_{\text{hyd}} = 10^{-2} \text{ m/s}$
Exponent	$\alpha = 3.0$

### Boundary conditions

The medium is subjected to a constant far-field vertical stress of  $\sigma_{z_\infty} = 1 \text{ MPa}$ . The initial lateral confining stress is  $\sigma_{x_\infty} = 1 \text{ MPa}$ ; after equilibration under the applied confinement, the medium is subjected to a zero horizontal displacement boundary condition for the fluid-injection stage. The bottom boundary allows for horizontal displacements only and the vertical displacement is zero. There is no flow across the lateral boundaries, and the pore pressure is constant at the top and bottom boundaries. An incompressible fluid is injected at a point located at the centreline, five layers above the rigid bottom boundary (Fig. 3(b)).

### Results

Numerical experiments show the role of the pre-structured medium in the evolution of block displacements (Fig. 4(a)). A preferential opening forms at the injection point and grows along the prevalent fabric direction in the blocky structure. Furthermore, there is extensive kinematic dilation away from the opening. The fluid pressure reflects the combination of two processes: (a) leak-off and advection away from the main opening – that is, pressure increases and (b) dilation and kinematic distortion in the fractured system, thus hindered fluid pressure increase where the fabric tends to dilate.

Figure 5(a) plots block displacement data along the centreline and above the injection point. The vertical displacement of the block 15 layers above the main opening is 35% higher than that at the main opening wall. Note that the stiffness-to-stress ratio is high in this numerical simulation ( $E/\sigma'_{z_0} = 1000$ ).

Figure 5(b) shows the change in mean stress inside the matrix. Blocks above the centreline bend with ends down, while blocks above the tip of the main opening deform upwards.

### ANALYSES AND DISCUSSION

The regular fabric of pre-structured media assumed in this study lends itself to simple geometrical analyses that provide insight into the evolution of the blocky formation during the generation of opening-mode discontinuities.

#### Wing openings

The inclination of wing openings with respect to the horizontal orientation can be expressed as a function of the block slenderness  $\lambda = L_b/H_b$  and the overlap ratio  $s/L_b$  (Fig. 1)

$$\beta = \arctan \left[ \frac{L_b}{H_b} \left( 1 - \frac{s}{L_b} \right) \right]^{-1} \quad (2)$$

The wing angle is  $\beta = 45^\circ$  for  $s/L_b = 0.5$ , and it reaches  $\beta = 79^\circ$  for  $s/L_b = 0.9$  ( $L_b/H_b = 2$ ). This geometric analysis assumes a stress-controlled upper boundary, and applies for any lateral boundary condition. Contiguous points on opposite faces of wing openings displace away from each other at an angle  $\chi = 90 - \beta$  with respect to the direction of the wing opening. For comparison, displacements are at  $\chi = 90^\circ$  in mode I fractures and at  $\chi = 0^\circ$  in mode II. These wing openings tend to remain propped open even after hydraulic fracturing, and become major conduits for fluid transport during production.

#### Fractures normal to the main opening

Experimental and numerical results presented above show the formation of the main opening-mode discontinuity and a concurrent network of secondary gaps that result from

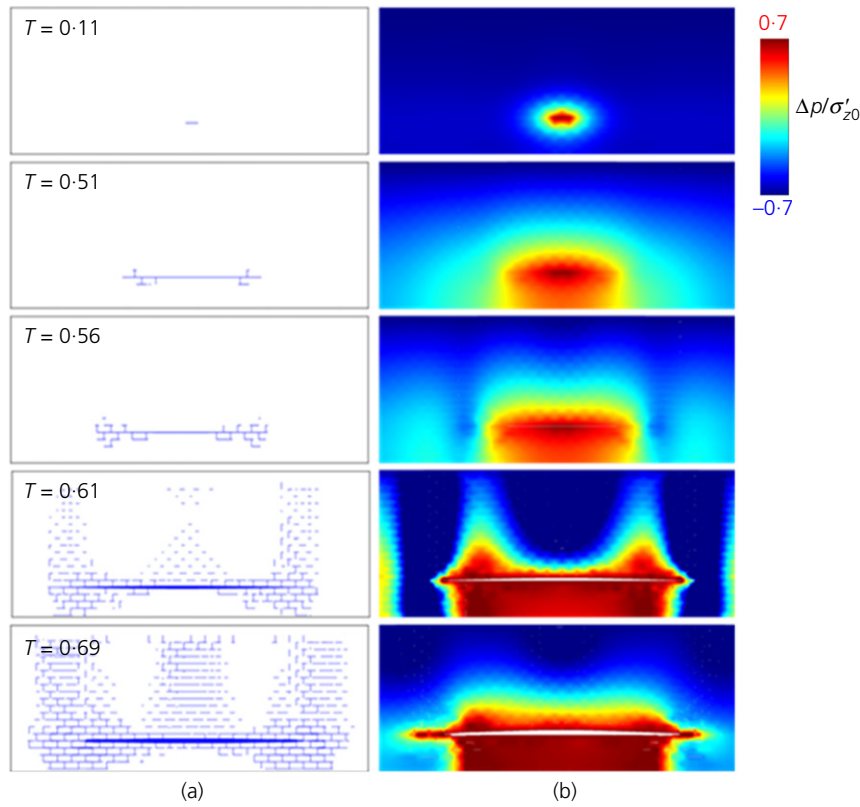


**Fig. 4.** Numerical simulation results – test conducted at a constant injection pressure equal to 1.4 times the overburden. (a) Fracture openings at different stages after the fluid injection starts (top to bottom); the line thickness is proportional to the aperture width. (b) Fluid pressure field corresponding to each stage after hydraulic fracture starts; the fluid pressure is normalised by the constant vertical stress applied on the upper boundary  $\Delta p/\sigma'_{z0}$ . Note: images in successive rows correspond to dimensionless times  $T = t \times c_{v\text{-frac}}/L_b^2 = 0.11, 0.51, 0.56, 0.61$  and  $0.69$

kinematic dilational distortion. The observed displacements take place even in the absence of tensile failures. The main opening involves a large number of blocks,  $L_F/L_b \gg 1$  (Fig. 6). The average aperture in fractures normal to the main opening is a function of the main opening width,  $O_F$  and length,  $L_F$ . Let us adopt a Pythagorean length

$$e = \frac{\Delta L}{N} \cong \frac{\sqrt{L_F^2 + O_F^2} - L_F}{L_F/L_b} \cong \frac{L_b}{2} \left( \frac{O_F}{L_F} \right)^2 \quad (3)$$

The simplified approximation obtained by Taylor expansion highlights the benefits of rounder openings – that is, larger  $O_F/L_F$  ratio. Consider a main fracture with  $L_F = 20$  m and  $O_F = 0.4$  m. On average, the aperture of transverse fractures will reach  $e = 0.2$  mm when blocks are  $L_b = 1$  m long. The evolution in fracture aperture reflects competing processes: (a) opening that results from the increased fluid pressure – that is, the injection rate is higher than the leak-off rate and (b) closing due to the expansion of nearby fractures. Pressure diffuses from the injection point into the formation before decisive opening-mode discontinuities start forming. The pressure required to open the main discontinuity is  $\sim 1.4$  times the overburden stress in numerical simulations.

Additional simulation results demonstrate that early fracture-opening trends are similar regardless of the exponent  $\alpha$  in the conductivity aperture, equation (1). However, the sensitivity of the hydraulic conductivity to the fracture aperture plays an important role in the evolution of fracturing and determines the final ‘plumbing’ topology. Block and fracture deformations (Figs 4 and 5) diminish dilational distortion at high stress because the work of dilation exceeds the energy required to break the rock at high effective stress.

Block splitting and corner crushing thus will hinder dilation. Still, even a limited dilational distortion can significantly enhance the permeability.

#### Enhanced conductivity in fractures normal to the main opening

Post-stimulation fluid transmissivity will reflect the consequences of kinematic dilation (Barton *et al.*, 1995; Dyke, 1995) and shear-induced dilation along critically stressed pre-existing fractures (Hossain *et al.*, 2002; Damjanac & Cundall, 2016; Liang *et al.*, 2016). Indeed, there will be a significant enhancement in fracture transmissivity (Zimmerman & Bodvarsson, 1996; Ito & Zoback, 2000; Johri & Zoback, 2013).

The conductivity  $k_{\text{hyd}}$  (m/s) of a rock mass is a function of the fracture aperture  $e$  (m) and spacing  $L_b$  (m), and the fluid unit weight ( $\text{kN/m}^3$ ) and viscosity  $\eta$  (Pa s) (Snow, 1965)

$$k_{\text{hyd}} = \frac{\gamma e^3}{6\eta L_b} \quad (4)$$

Equations (3) and (4) combine to highlight the strong effect that the main opening roundness  $O_F/L_F$  has on the rock mass conductivity contributed by the transverse fractures

$$k_{\text{hyd}} = \frac{\gamma L_b^2}{48\eta} \left( \frac{O_F}{L_F} \right)^6 \quad (5)$$

#### CONCLUSIONS

High-pressure fluid injection in pre-structured media can cause opening-mode discontinuities that are distinct from hydraulic fractures in homogeneous cohesive media

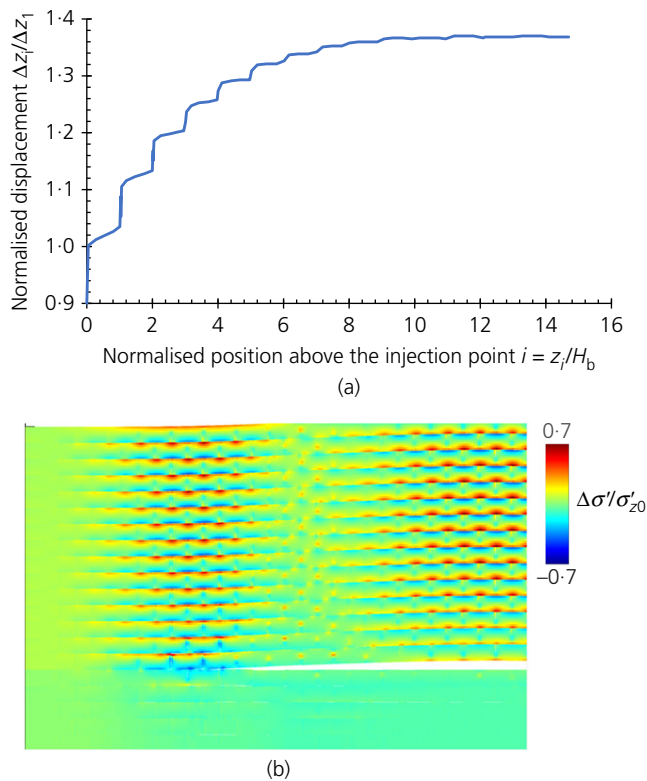


**Fig. 5.** Numerical simulation results: dilational distortion. Test conducted at a constant injection pressure equal to 1.4 times the overburden. (a) Layer displacement normalised by the displacement at the main opening  $\Delta z/\Delta z_1$  against position above the injection point normalised by the block height  $i = z/H_b$ . (b) Change in induced mean stress inside blocks (red: compression, blue: tension)

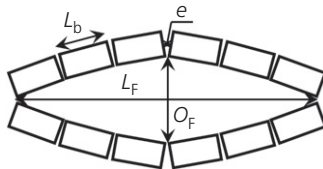


**Fig. 6.** Main opening roundness  $O_F/L_F$  and aperture width of fractures normal to the main opening

(e.g. intact rocks), or in frictional uncemented granular media (i.e. soils). In particular, the internal structure-dependent kinematic dilation emerges as an inherent response of pre-fractured media. Parameters such as block size, block slenderness and inter-block overlap length characterise pre-structured media and strongly affect the formation of opening-mode discontinuities.

The internal structure (a) biases the initiation of the opening along the prevalent fabric orientation, rather than normal to the minimum principal stress, (b) determines the formation of either wing openings for short block overlap or vertical displacement along columnar structures for long block overlap and (c) affects the injection pressure required to initiate the main opening. In fact, the pressure required to disturb a blocky medium can be much higher than the overburden due to interlocking.

Geometric distortion and dilation of the internal blocky structure are extensive around the main opening. The work of dilation against the confining stress increases with depth. Eventually, block deformation, splitting or edge crushing gain relevance; thus, dilation should decrease with depth.

Kinematically admissible dilational distortion has a profound effect on fluid conductivity in the pre-fractured medium. In theory, one can anticipate a six-power relationship between the main opening roundness and the equivalent hydraulic conductivity of the rock mass in the direction normal to the main opening (equation (5)).

Frictional self-propping locks-in dilational distortion and maintains a high hydraulic conductivity after depressurisation. Self-propping develops more readily in rounder main openings as predicted by equation (5). High fluid flow rates and high viscosities favour the creation of rounder main openings.

The stimulation of pre-fractured, structured reservoirs does not require the tensile failure of rock blocks. Furthermore, dilational distortion extends the stimulated zone away from the main opening to zones not reached by the injection fluid pressure. These observations inform the interpretation of seismic events; in particular, the association between the stimulated reservoir volume and the volume defined by seismic events require careful consideration.

#### ACKNOWLEDGEMENTS

Support for this research was provided by the US Department of Energy and the King Abdullah University of Science and Technology endowment. G. Abelskamp edited the manuscript.

#### REFERENCES

- Barton, N., Bandis, S. & Bakhtar, K. (1985). Strength, deformation and conductivity coupling of rock joints. *Int. J. Rock Mech. Min. Sci.* **22**, No. 3, 121–140.
- Barton, C. A., Zoback, M. D. & Moos, D. (1995). Fluid flow along potentially active faults in crystalline rock. *Geology* **23**, No. 8, 683–686.
- Chen, Z., Narayan, S. P., Yang, Z. & Rahman, S. S. (2000). An experimental investigation of hydraulic behaviour of fractures and joints in granitic rock. *Int. J. Rock Mech. Min. Sci.* **37**, No. 7, 1061–1071.
- Cheng, W., Jin, Y. & Chen, M. (2015). Reactivation mechanism of natural fractures by hydraulic fracturing in naturally fractured shale reservoirs. *J. Nat. Gas Sci. Engng* **27**, No. 3, 1357–1365.
- Cooke, M. L. & Underwood, C. A. (2001). Fracture termination and step-over at bedding interfaces due to frictional slip and interface opening. *J. Struct. Geol.* **23**, 223–238.
- Dahi-Taleghani, A. & Olson, J. E. (2011). Numerical modeling of multistranded-hydraulic-fracture propagation: accounting for the interaction between induced and natural fractures. *AAPG Bull.* **16**, No. 3, 575–581.
- Damjanac, B. & Cundall, P. (2016). Application of distinct element methods to simulation of hydraulic fracturing in naturally fractured reservoirs. *Comput. Geotech.* **71**, 283–294.
- Daneshy, A. A. (1974). Hydraulic fracture propagation in the presence of planes of weakness. *SPE European Spring Meeting*. Amsterdam, Netherlands: Society of Petroleum Engineers, Richardson, TX, USA.
- Delaguna, W. (1966). Disposal of radioactive wastes by hydraulic fracturing. 2-Mechanics of fracture formation and design of observation and monitoring wells. *Nucl. Engng Des.* **3**, No. 3, 432–438.
- De Pater, C. J. & Beugelsdijk, L. J. L. (2005). Experiments and numerical simulation of hydraulic fracturing in naturally fractured rock. *The 40th U.S. symposium on rock mechanics (USRMS)*, rock mechanics for energy, mineral and infrastructure development in the Northern regions; Alaska rocks (ed. G. Chen), pp. 1–12. Anchorage, Alaska, USA: American Rock Mechanics Association.
- Detournay, E. (2016). Mechanics of hydraulic fractures. *Annu. Rev. Fluid Mech.* **48**, 311–339.
- Dyke, C. G. (1995). How sensitive is natural fracture permeability at depth to variation in effective stress? *Fractured and jointed rock masses*. The international ISRM symposium on fractured and

- jointed (ed. A. A. Balkema). Rotterdam, the Netherlands: Balkema.
- Economides, M. J. & Nolte, K. G. (2000). *Reservoir stimulation*. New York, USA: Wiley.
- Gale, J. F. W., Reed, R. M. & Holder, J. (2007). Natural fractures in the Barnett shale and their importance for hydraulic fracture treatments. *AAPG Bull.* **91**, No. 4, 603–622.
- Garcia, A., Rached, R. & Santamarina, J. C. (2018). Hydraulic fracturing in pre-fractured media. *International symposium on energy geotechnics SEG 2018, Lausanne, Switzerland*.
- Haimson, B. & Fairhurst, C. (1969). *In situ stress determination at great depth by means of hydraulic fracturing, The 11th U.S. Symposium on Rock Mechanics (USRMS)*, Berkeley, California, USA. American Rock Mechanics Association.
- Hossain, M. M., Rahman, M. K. & Rahman, S. S. (2002). A shear dilation stimulation model for production enhancement from naturally fractured reservoirs. *SPE J.* **7**, No. 2, 183–195.
- Hubbert, M. K. & Willis, D. G. (1957). Mechanics of hydraulic fracturing. *Trans. Am. Inst. Min. Metall. Engrs* **210**, No. 6, 153–163.
- Ito, T. & Zoback, M. D. (2000). Fracture permeability and in situ stress. *Geophys. Res. Lett.* **27**, No. 7, 1045–1048.
- Jeffrey, R. G., Zhang, X. & Bungler, A. P. (2010). *Hydraulic fracturing of naturally fractured reservoirs*. Stanford, CA, USA: Stanford Geothermal Program, pp. 289–297.
- Johri, M. & Zoback, M. D. (2013). The evolution of stimulated reservoir volume during hydraulic stimulation of shale gas formations. *Unconventional resources technology conference*, Denver, Colorado, USA, URTeC 1575434.
- Lakirouhani, A., Detournay, E. & Bungler, A. (2016). A reassessment of in situ stress determination by hydraulic fracturing. *Geophys. J. Int.* **205**, No. 3, 18591873.
- Lam, K. Y. & Cleary, M. P. (1984). Slippage and re-initiation of (hydraulic) fractures at frictional interfaces. *Int. J. Numer. Anal. Methods Geomech.* **8**, No. 6, 589–604.
- Lamont, N. & Jessen, F. W. (1963). The effects of existing fractures in rocks on the extension of hydraulic fractures. *Trans. Soc. Petrol. Engrs AIME* **228**, No. 2, 203–209.
- Last, N. C. & Harper, T. R. (1990). Response of fractured rock subject to fluid injection. 1. Development of a numerical model. *Tectonophysics* **172**, No. 1–2, 1–31.
- Lee, H. P., Olson, J. E., Holder, J., Gale, J. F. W. & Myers, R. D. (2015). The interaction of propagating opening mode fractures with preexisting discontinuities in shale. *J. Geophys. Res.: Solid Earth* **120**, No. 1, 169–181.
- Lei, Q., Latham, J. P., Xiang, J. & Tsang, C. F. (2015). Polyaxial stress-induced variable aperture model for persistent 3D fracture networks. *Geomech. Energy Environ.* **1**, 3447.
- Liang, B., Jiang, H., Li, J. & Gong, C. (2016). A systematic study of fracture parameters effect on fracture network permeability based on discrete-fracture model employing finite element analyses. *J. Nat. Gas Sci. Engng* **28**, 711–722.
- Maxwell, S. C., Cho, D., Pope, T., Jones, M., Cipolla, C., Mack, M., Henery, F., Norton, M. & Leonard, J. (2011). Enhanced reservoir characterization using hydraulic fracture microseismicity. *SPE hydraulic fracturing technology conference and exhibition*, Woodlands, Texas, USA: Society of Petroleum Engineers, pp. 457–467.
- Mayerhofer, M. J., Richardson, M. F., Walker, R. N., Meehan, D. N., Oehler, M. W. & Browning, R. R. (1997). Proppants? We don't need no proppants. *SPE-38611-MS, SPE annual technical conference and exhibition*, pp. 457–464. San Antonio, Texas, USA: Society of Petroleum Engineers.
- Mayerhofer, M. J., Stegent, N. A., Barth, J. O. & Ryan, K. M. (2011). Integrating fracture diagnostics and engineering data in the Marcellus shale. *SPE annual technical conference and exhibition*, Denver, Colorado, USA: Society of Petroleum Engineers, pp. 518–532.
- NAE (National Academy of Engineering) (2015). *Characterization, modeling, monitoring, and remediation of fractured rock*. Washington, DC, USA: The National Academies Press.
- Nagel, N. B., Sanchez-Nagel, M. A., Zhang, F., Garcia, X. & Lee, B. (2013). Coupled numerical evaluations of the geomechanical interactions between a hydraulic fracture stimulation and a natural fracture system in shale formations. *Rock Mech. Rock Engng* **46**, No. 3, 581–609.
- Ren, L., Su, Y., Zhan, S., Hao, Y., Meng, F. & Sheng, G. (2016). Modeling and simulation of complex fracture network propagation with SRV fracturing in unconventional shale reservoirs. *J. Nat. Gas Sci. Engng* **28**, 132–141.
- Riahi, A., Damjanac, B. & Furtney, J. (2014). *Thermo-hydro-mechanical numerical modeling of stimulation and heat production of EGS reservoirs, 48th U.S. Rock Mechanics/ Geomechanics Symposium, Minneapolis, Minnesota, USA*. American Rock Mechanics Association.
- Segura, J. M. & Carol, I. (2008). Coupled HM analysis using zero-thickness interface elements with double nodes. Part I: theoretical model. *Int. J. Numer. Anal. Methods Geomech.* **32**, No. 18, 2083–2101.
- Shin, H. & Santamarina, J. C. (2008). Fluid-driven fractures in un cemented sediments: underlying particle-level processes. *Earth Planet. Sci.* **299**, No. 1–2, 180–189.
- Snow, D. T. (1965). *A parallel plate model of fractured permeable media*. PhD dissertation, University of California, Berkeley, CA, USA.
- Souley, M., Lopez, P., Boulon, M. & Thoraval, A. (2015). Experimental hydromechanical characterization and numerical modelling of a fractured and porous sandstone. *Rock Mech. Rock Engng* **48**, No. 3, 1143–1161.
- Teufel, L. W. & Clark, J. A. (1984). Hydraulic fracture propagation in layered rock – experimental studies of fracture containment. *Soc. Petrol. Engrs J.* **24**, No. 1, 19–32.
- Thiercelin, M., Roegiers, J. C., Boone, T. J. & Ingraffea, A. R. (1987). An investigation of the material parameters that govern the behavior of fractures approaching rock interfaces. *6th international congress of rock mechanics*, Montreal, Canada: International Society for Rock Mechanics and Rock Engineering, pp. 263–269.
- Tsang, C. F., Neretnieks, I. & Tsang, Y. (2015). Hydrologic issues associated with nuclear waste repositories. *Environ. Earth Sci.* **51**, No. 9, 6923–6972.
- Wang, H. Y. (2017). What Factors Control Shale-Gas Production and Production-Decline Trend in Fractured Systems: A Comprehensive Analysis and Investigation. *SPE Journal* **22**, 562–581.
- Warpinski, N. R. & Teufel, L. W. (1987). Influence of geologic discontinuities on hydraulic fracture propagation. *J. Petrol. Technol.* **39**, No. 2, 209–220.
- Warpinski, N. R., Mayerhofer, M. J., Vincent, M. C., Cipolla, C. L. & Lolon, E. P. (2009). *Stimulating unconventional reservoirs: maximizing network growth while optimizing fracture conductivity*. Richardson, TX, USA: Society of Petroleum Engineers, p. 114173.
- Wasantha, P. L. P. & Konietzky, H. (2016). Fault reactivation and reservoir modification during hydraulic stimulation of naturally fractured reservoirs. *J. Nat. Gas Sci. Engng* **34**, 908–916.
- Zhang, X., Jeffrey, R. G. & Thiercelin, M. (2009). Mechanics of fluid-driven fracture growth in naturally fractured reservoirs with simple network geometries. *J. Geophys. Res. – Solid Earth* **114**, No. 12, 16.
- Zhou, J., Chen, M., Jin, Y. & Zhang, G. (2008). Analysis of fracture propagation behavior and fracture geometry using a tri-axial fracturing system in naturally fractured reservoirs. *Int. J. Rock Mech. Min. Sci.* **45**, 1143–1152.
- Zimmerman, R. W. & Bodvarsson, G. S. (1996). Hydraulic conductivity of rock fractures. *Transp. Porous Media* **23**, No. 1, 1–30.
- Zoback, M. D., Rummel, F., Jung, R. & Raleigh, C. B. (1977). Laboratory hydraulic fracturing experiments in intact and prefractured rock. *Int. J. Rock Mech. Min. Sci.* **14**, No. 2, 49–58.
- Zoback, M. D., Fuchs, K., Rummel, F. & Baumgartner, J. (2003). Estimation of the complete stress tensor to 8 km depth in the KTB scientific drill holes: implications for crustal strength. *J. Geophys. Res. – Solid Earth* **102**, No. B8, 18453–18475.

#### HOW CAN YOU CONTRIBUTE?

To discuss this paper, please submit up to 500 words to the editor at journals@ice.org.uk. Your contribution will be forwarded to the author(s) for a reply and, if considered appropriate by the editorial board, it will be published as a discussion in a future issue of the journal.